# Nonlinear semi-numeric analysis and simplified analysis of polymer fiber-reinforced concrete prisms under three-point bending test conditions

*Ziga* Unuk[1*]

[1]Faculty of Civil Engineering, Transportation Engineering and Architecture, University of Maribor, Smetanova ulica 17, 2000 Maribor, Slovenia

**Abstract.** This paper presents a semi-numeric nonlinear analysis and a simplified analysis for evaluating the load-displacement behavior of polymer fiber-reinforced concrete elements under three-point bending test conditions. The considered elements were notched and unnotched prisms. The nonlinear semi-numeric analysis was based on the moment-curvature relation, plastic hinge approach, and virtual work method. The simplified analysis assumed multilinear load-displacement behavior of the prisms under three-point bending test conditions. It included four variants for the input tensile strength properties and crack widths considered for the serviceability and ultimate limit state. The notched polymer fiber-reinforced concrete prism three-point bending test results from a prior study were the basis for evaluating the simplified analysis, which was subsequently compared with the nonlinear semi-numeric analysis outcomes from the same investigation. Additionally, the simplified analysis and the nonlinear semi-numeric analysis were used to determine the load-displacement behavior of unnotched polymer fiber-reinforced concrete prisms with heights ranging from 25 mm to 250 mm. The results indicate that the simplified analysis provides a practical and efficient method for estimating the behavior of polymer fiber-reinforced concrete structures under three-point bending test conditions, yielding relatively accurate results with minimal computational effort compared to the more exact nonlinear semi-numeric analysis.

## 1 Introduction

Polymer fiber-reinforced concrete is increasingly used in modern construction due to its enhanced mechanical properties, durability, and resistance to various environmental factors. Its applications span across several areas of construction, for example, concrete pavements [1], bridge decks [2], pre-cast sleeper elements [3] and shotcrete applications in tunnel linings [4]. Applying a uniform tensile force to structural elements composed of fiber-reinforced concrete results in a nonlinear load-displacement response, and this non-linearity is significantly increased under bending loads.

* Corresponding author: ziga.unuk@um.si

Various computational methods have been formulated to represent fiber-reinforced concrete's highly nonlinear load-displacement characteristics accurately. As noted in [5], the plastic hinge method (or variations of it) is among the most frequently utilized techniques for computationally describing the nonlinear load-displacement behavior (see, for example, the studies [6], [7], [8], [9] and [10]). Certain studies also focus on describing the load-displacement behavior of fiber-reinforced concrete elements by (relatively) more simplified methods. In the study [11], a semi-analytical model is introduced to assess the bending behavior of fiber-reinforced concrete, calculating midspan displacement by adding the displacement from classical beam theory to the displacement resulting from rotation at a crack. This rotation was determined by dividing the crack width by the crack depth. In [12], the midspan deflection of fiber-reinforced beams under four-point bending test conditions was calculated by multiplying the midspan (cracked) cross-section rotation with half of the span length. The rotation was calculated by integrating the axial strain (calculated by a sectional analysis) at the top fiber over the whole beam length and using simplified geometric relations. Most research on fiber-reinforced concrete focuses on rectangular cross-sections; however, the study [13] explored the load-bearing behavior of tetrapods, four legged elements with circular cross-sections, made from polymer fiber-reinforced concrete.

Current methods for simulating the load-displacement behavior of fiber-reinforced concrete elements under bending, despite their varying levels of simplification, demand significant computational effort. A more simplified model that can relatively accurately estimate this behavior with minimal computational effort would enhance the design and analysis process for fiber-reinforced concrete structures in a preliminary design phase, for example, to determine the required concrete composition. This study, therefore, focuses on a simplified analysis of the load-displacement behavior of previously tested notched polymer fiber-reinforced concrete prisms. It builds on the previous study [14], where three-point bending tests of notched polymer fiber-reinforced concrete prisms were performed and analyzed by a nonlinear semi-numeric analysis – while the nonlinear semi-numeric analysis resulted in load-displacement relations, which matched the averaged experimental results, the calculation showed to be tedious in terms of engineering practice. In addition to the analysis of the notched prisms, multiple unnotched concrete prism geometries (by varying the cross-section height) were analyzed by the nonlinear semi-numeric analysis (presented in [14]) and the simplified analysis. Different variants for determining the input material properties were considered for the simplified analysis. The simplified analysis results were compared to the more exact results of the nonlinear semi-numeric analysis to assess the different variants for determining the input material properties and the overall effectiveness of the simplified analysis.

## 2 Analysis of three-point bending tests of notched polymer fiber-reinforced concrete prisms

The analyzed prisms had a length of 600 mm and a rectangular cross-section with a nominal height ($h$) and nominal width ($b$) of 150 mm (see Fig. **1**). The prisms were notched at the midspan. The notched cross-section height ($h_{sp}$) was 125 mm. The span length ($L$) was 500 mm. The exact concrete composition, which can be found in [14], was designed to reach a characteristic compressive strength (on cylinders, according to the EN1992-1-1 standard [15]) of at least 25 MPa, respectively, the properties of strength class C25/30. In addition to the regular concrete components, 5 kg of the Barchip 48 [16] polymer fibers were added per cubic meter of the concrete composition. They can be classified as Class-II fibers (according to the EN 14889-2 standard [17]), generally used where an increase in residual flexural strength is required.

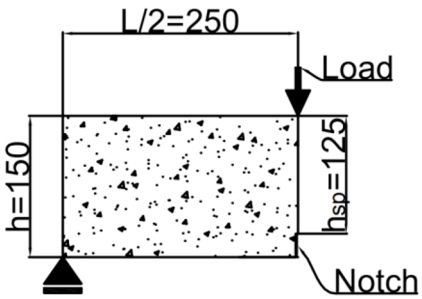


**Fig. 1.** The analyzed notched polymer fiber reinforced concrete prisms with the load test configuration (only half of the model is shown as it is symmetric).

## 2.1 Nonlinear Semi-Numeric Analysis

The semi-numeric nonlinear procedure is presented in detail in [14] and is only briefly outlined herein. The nonlinear semi-numeric analysis (load-displacement relation calculation) was based on the moment-curvature relation, plastic hinge approach, and virtual work method. The fiber-reinforced concrete constitutive model from the fib Model Code for Concrete Structures 2010 [18] (see Fig. **2**) was considered. The constitutive model was modified to consider the crack tip opening displacement (CTOD) as the crack widths, not the crack mouth opening displacement (CMOD) as proposed by the fib Model Code for Concrete Structures 2010 [18]. Note that a value of 1.2 is accepted for the ratio CMOD/CTOD.

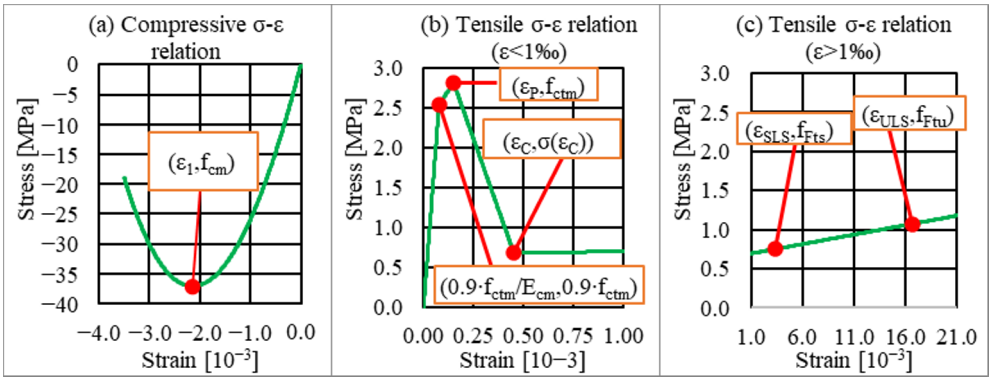


**Fig. 2.** Constitutive law of fiber-reinforced concrete according to the fib Model Code for Concrete Structures 2010 [18] (the graphs have different scales for clarity): (a) in compression; (b) in tension for small strains of < 1‰; and (c) in tension for large strains of > 1‰.

The tensile mechanical properties were evaluated through a reverse analysis (an inverse analysis) of the three-point bending tests, while additional mechanical properties were ascertained through compressive testing and established correlations between the compressive strength and other various mechanical properties of concrete. The concrete properties determined and used for the calculation are collected in Table 1. Note that the strain values for fiber-reinforced concrete depend on the notched cross-section height (125 mm).

**Table 1.** Considered fiber-reinforced concrete properties (from [14]).

| Property | Property designation | Unit | Value |
|---|---|---|---|
| Compressive strength | $f_{cm}$ | [MPa] | 37.10 |
| Modulus of elasticity | $E_{cm}$ | [GPa] | 32.60 |
| Strain at the maximum compressive stress | $\varepsilon_{c1}$ | [$10^{-3}$] | −2.15 |
| Fracture energy of plain concrete | $G_F$ | [N/m] | 139.90 |
| Strain corresponding to the tensile strength | $\varepsilon_P$ | [$10^{-3}$] | 0.15 |
| Tensile strain at which the tensile behavior starts to differ from the plain concrete behavior | $\varepsilon_C$ | [$10^{-3}$] | 0.45 |
| Limit tensile strain of fiber-reinforced concrete for the serviceability limit state | $\varepsilon_{SLS}$ | [$10^{-3}$] | 3.33 |
| Limit tensile strain of fiber-reinforced concrete for the ultimate limit state | $\varepsilon_{ULS}$ | [$10^{-3}$] | 16.67 |
| Tensile strength | $f_{ctm}$ | [MPa] | 2.82 |
| Fiber-reinforced concrete residual tensile strength for the serviceability limit state | $f_{Fts}$ | [MPa] | 0.75 |
| Fiber-reinforced concrete residual tensile strength for the ultimate limit state | $f_{Ftu}$ | [MPa] | 1.07 |

## 2.2 Simplified analysis

Polymer fiber-reinforced elements typically show tensile softening behavior under bending loads, where most deformation results from one crack, which forms at the location of the maximum load. Accordingly, the simplified analysis of the three-point bending tests of notched polymer fiber-reinforced concrete prisms assumed that the load-displacement relation can be described by three pairs of loads and corresponding displacements (coordinate pairs on a load-displacement chart):

- the maximum load and the corresponding displacement (Point 1);
- the load corresponding to the serviceability limit state and the corresponding displacement (Point 2);
- the load corresponding to the ultimate limit state and the corresponding displacement (Point 3).

The complete multilinear load-displacement relation (see Fig. **3**) is then established by connecting the coordinate origin (as the starting point of the load-displacement relation) and point 1. The next step is to connect point 2 and point 3. After reaching the maximum load, the load is assumed to decrease with the constant displacement corresponding to the maximum load. The load is assumed to decrease until it reaches the intersection with the line connecting points 2 and 3 (the line is extended until it intersects with the vertical line at the displacement corresponding to the maximum load).

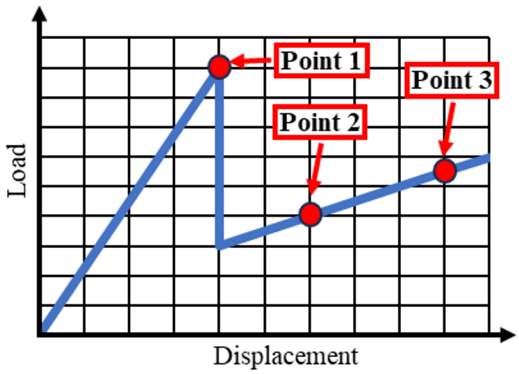


**Fig. 3.** Simplified load-displacement behavior of the polymer fiber-reinforced prisms under three-point bending test conditions.

The maximum load was calculated as the product of the concrete flexural strength and section modulus of the rectangular (notched) cross-section. The corresponding midspan vertical displacement is calculated as the sum of the bending deflection of the beam with the gross cross-section (unnotched), the shear deflection and the bending deflection due to the notched cross-section. The elastic bending deflection ($\Delta_{b.g}$) of the beam with the gross cross-section (unnotched) is calculated with:

$$\Delta_{b.g} = \frac{F \cdot L^3}{48 \cdot E_{cm} \cdot I}, \quad (1)$$

where $F$ is the considered load, $L$ is the span length and $I$ is the moment of inertia of the gross cross-section. The elastic shear deflection is calculated with:

$$\Delta_s = \frac{F \cdot L \cdot (1+\nu)}{2 \cdot E_{cm} \cdot b \cdot h \cdot \kappa_s}, \quad (2)$$

where $\nu$ is the Poisson coefficient for concrete (equal to 0.2) and $\kappa_s$ is the shear correction factor for rectangular cross-sections (equal to 5/6). The bending deflection due to the notched cross-section was calculated with the expression from [19]:

$$\Delta_{b.n} = \frac{3 \cdot F \cdot L^2}{2 \cdot E_{cm} \cdot b \cdot h^2} \cdot (5.58 - 19.57 \cdot r + 36.82 \cdot r^2 - 34.94 \cdot r^3 + 12.77 \cdot r^4), \quad (3)$$

where $r$ is the ratio $(h-h_{sp})/h$. The total deflection corresponding to the maximum load (and lower loads on the line between the chart origin and Point 1) is the sum of deflections $\Delta_{b.g}$, $\Delta_s$ and $\Delta_{b.n}$.

For calculating the loads corresponding to the serviceability limits state and the ultimate limit state, simplified normal stress distributions from the fib Model Code for Concrete Structures 2010 [18] were considered. For the serviceability limit state, the behavior of fiber-reinforced concrete is described as elastoplastic in tension and elastic in compression, with maximum compressive stress equal to $\sigma$ (Fig. **4** a)). For the ultimate limits state, it is considered that the compressive stress in the cross-section is concentrated at the compressed edge (as force $C$) and that the tensile stress varies linearly between $f_{Fts}$ (at the compressed

cross-section edge) and $f_{Ftu}$ (at the tensioned cross-section edge) (Fig. **4** b)). A more detailed explanation is given in [20].

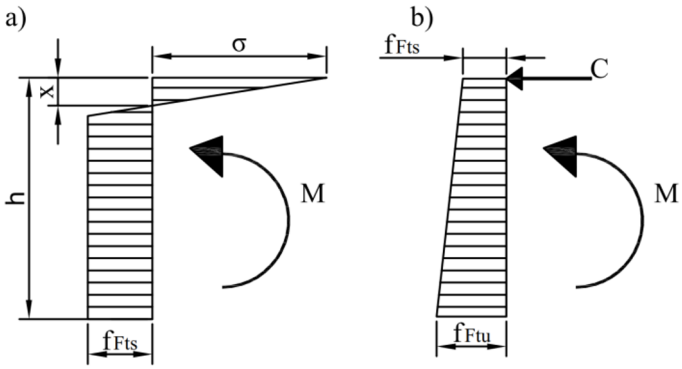


**Fig. 4.** Simplified normal stress distributions: a) for the serviceability limit state, b) for the ultimate limit state (adapted from the fib Model Code for Concrete Structures 2010 [18]).

For the serviceability limit state (the considered stress distribution is given in Fig. **4** a)), based on the equilibrium conditions for axial forces, the compression zone height $x$ can be calculated with:

$$x = \frac{f_{Fts}^{\,2} \cdot h_{sp}^{\,3} + E_{cm} \cdot w_s \cdot \sqrt{2 \cdot E_{cm} \cdot f_{Fts} \cdot h_{sp}^{\,3} \cdot w_s - f_{Fts}^{\,2} \cdot h_{sp}^{\,4}} - 2 \cdot E_{cm} \cdot f_{Fts} \cdot h_{sp}^{\,2} \cdot w_s}{(E_{cm} \cdot w_s - f_{Fts} \cdot h_{sp})^2}, \tag{4}$$

where $f_{Fts}$ is the fiber-reinforced concrete residual tensile strength for the serviceability limit state and $w_s$ is the crack width for the serviceability limit state. The equilibrium of bending moments is given with:

$$M = \frac{b \cdot f_{Fts} \cdot (h_{sp} - x) \cdot (3 \cdot E_{cm}^{\,2} \cdot h_{sp} \cdot w_s^{\,2} + x \cdot E_{cm}^{\,2} \cdot w_s^{\,2} - 2 \cdot x \cdot E_{cm} \cdot f_{Fts} \cdot h_{sp} \cdot w_s - f_{Fts}^{\,2} \cdot h_{sp}^{\,3} + x \cdot f_{Fts}^{\,2} \cdot h_{sp}^{\,2}}{6 \cdot E_{cm}^{\,2} \cdot w_s^{\,2}}. \tag{5}$$

For the ultimate limit state (Fig. **4** b)), the equilibrium of bending moments is given with:

$$M = f_{Ftu} \cdot \frac{b \cdot h_{sp}^{\,2}}{2} + (f_{Fts} - f_{Ftu}) \cdot \frac{b \cdot h_{sp}^{\,3}}{3}. \tag{6}$$

where $f_{Ftu}$ is the fiber-reinforced concrete residual tensile strength for the ultimate limit state.

For the serviceability limit state and the ultimate limit state, the total deflection was assumed to be a sum of the elastic bending deflection ($\Delta_{b.g}$) of the beam with the gross cross-section (unnotched), the elastic shear deflection ($\Delta_s$) and the deflection due to the rotation at the crack cross-section ($\Delta_{\varphi.i}$). For the serviceability limit state, it is assumed that the prism rotates around the point with zero strain at the cracked cross-section. In contrast, for the ultimate limit state, it is assumed that the prism rotates around the cracked cross-section's top (compressed) edge (see Fig. **5**).

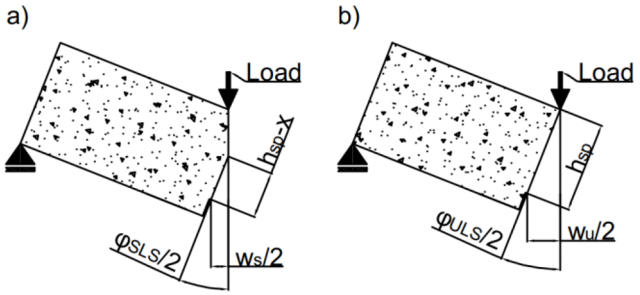


**Fig. 5.** Simplified models for calculating the rotation at the notch (or crack): a) for the serviceability limit state, b) for the ultimate limit state (only half of the models are shown as they are symmetric).

The cracked cross-section rotation for the serviceability limit state is calculated with:

$$\varphi_{SLS} = 2 \cdot asin\left(\frac{w_s}{2 \cdot (h_{sp} - x)}\right), \tag{7}$$

while for the ultimate limit state, the rotation is calculated with:

$$\varphi_{ULS} = 2 \cdot asin\left(\frac{w_u}{2 \cdot h_{sp}}\right), \tag{8}$$

where $w_u$ is the crack width considered for the ultimate limit state.

The deflection due to the cracked cross-section rotation ($\Delta_{\varphi.i}$), is calculated with:

$$\Delta_{\varphi.i} = \frac{L}{2} \cdot sin\left(\frac{\varphi_i}{2}\right). \tag{9}$$

Four combinations (variants) of the tensile strength properties (tensile strength of the concrete $f_{ctm}$ and the residual strengths $f_{Fts}$ and $f_{Ftu}$) and crack width values were considered for the simplified analysis.

The first variant (V1) considered the tensile strengths properties determined by the inverse analysis of the experimental results (given in Table 1) and crack tip opening displacement values (CTOD) as the crack widths (contrary to fib Model Code for Concrete Structures 2010 [18] which considers the crack mouth opening displacement values (CMOD) as the crack width). For the serviceability limit state, the crack width was equal to 0.42 mm; for the ultimate limit state, it was equal to 2.08 mm.

The second variant (V2) considered the tensile strength properties determined by simplified expressions from the fib Model Code for Concrete Structures 2010 [18]. The average experimentally determined flexural tensile strength ($f_{fl}$, equal to 4.52 MPa, see study [14]) was used to calculate the tensile strength of concrete ($f_{ctm}$) with the relation:

$$f_{ctm} = f_{fl} \cdot \frac{0.06 \cdot h_{sp}^{0.7}}{1 + 0.06 \cdot h_{sp}^{0.7}}. \tag{10}$$

Note that the same relation was used to calculate the flexural tensile strength from the tensile strength (from Table 1) for Variant 1 (V1). The residual tensile strength for the

serviceability limit state and ultimate limit state were calculated by simplified expressions (as per [18]):

$$f_{Fts}=0.45 \cdot f_{R1} \tag{11}$$

and

$$f_{Ftu}=0.5 \cdot f_{R3}-0.2 \cdot f_{R1}, \tag{12}$$

where $f_{R1}$ is the experimentally determined residual flexural tensile strength for the CMOD value of 0.5 mm (considered for the serviceability limit state and equal to 2.09 MPa, as experimentally determined in the study [14]) and $f_{R3}$ is the experimentally determined residual flexural tensile strength for the CMOD value of 2.5 mm (considered for the ultimate limit state and equal to 2.69 MPa, as experimentally determined in the study [14]). Variant 2 (V2) also considered the crack tip opening displacement values (CTOD) as the crack widths.

Variant 3 (V3) was similar to Variant 2, but it considered the CMOD values as the crack widths (0.5 mm for the SLS and 2.5 mm for the ULS).

Variant 4 (V4) considered the same flexural tensile strength as Variant 2. However, the residual tensile strength values $f_{Fts}$ and $f_{Ftu}$ were calculated by fapplying Equations 4, 5 and 6 (by equating the external bending moments to the experimental results (products of $f_{R1}$ or $f_{R3}$ and the section modulus of the cross-section). The Variant 4 (V4) also considered the crack tip opening displacement values (CTOD) as the crack widths.

### 2.3 Notched prisms: results and comparison

The results of the nonlinear semi-numeric analysis and the simplified analysis are collected in the form of load-displacement charts in Fig. **6**. In addition to calculation results, experimental results from the study [14], in form of averaged and envelope results, are given. In Fig. **6**, vertical displacement values are marked, which, according to the EN14651 standard [21], correspond to the CMOD (and CTOD) values of interest. The vertical displacement of 0.47 mm corresponds to the CMOD value of 0.5 mm and the vertical displacement of 2.17 mm corresponds to the CMOD value of 2.5 mm (these displacement values are considered for determining the load-bearing capacities for the serviceability and ultimate limit state). The results in the post-crack region are therefore evaluated regarding those two points (displacements and loads). The nonlinear semi-numeric analysis results matched the averaged experimental results and, as discussed in [14], proved to be a tool for relatively exact determination of the load-displacement behavior of fiber-reinforced concrete elements.

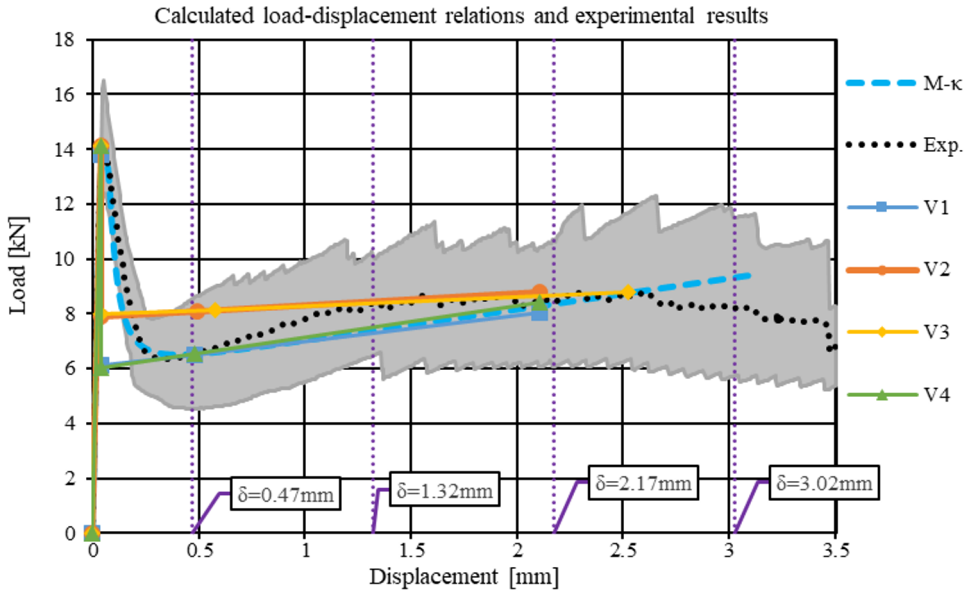


**Fig. 6.** Results of the simplified analysis (four Variants, V1–V4), nonlinear semi-numeric analysis (M-κ) and averaged experimental results (Exp.) (the shaded area represents the envelope of all experimental results).

The results in Fig. **6** show that the simplified analysis results match the experimental results in the "pre-crack" region of the load-displacement chart (from chart origin to Point 1 in terms of the simplified analysis in Fig. **3**). However, for the post-crack region (after reaching the maximum load) between displacements of 0.47 mm and 2.17 mm, only the simplified analysis with properties according to variants V1 and V4 gives results close to the averaged experimental and nonlinear semi-numeric analysis results. In comparison, Variant 2 is only close to the averaged experimental and nonlinear semi-numeric analysis results at the displacement of 2.17 mm. Variant 3 seems to be the least accurate, a direct consequence of using CMOD values for the crack widths. The most problematic region (in the sense of matching results) of the simplified analysis results is the post-crack region up to displacements of 0.47 mm. However, this region (also called transition region), where the fiber action starts to dominate the load-bearing behavior, is not of particular interest for the design of fiber-reinforced concrete elements.

Table 2 gives the load-displacement results at the points of interest (Point 1-3 in terms of Fig. **3**). MAX denotes the maximum load and corresponding displacement (Point 1), SLS denotes the serviceability limit state load and displacement (Point 2) and ULS denotes the ultimate limit state load and displacement (Point 3).

**Table 2.** Notched prisms: results of the simplified analysis (four Variants, V1–V4), nonlinear semi-numeric analysis (M-κ) and averaged experimental results (Exp.).

| | **V1** | | **V2** | | **V3** | | **V4** | | **M-κ (from [14])** | | **Exp. (from [14])** | |
|---|---|---|---|---|---|---|---|---|---|---|---|---|
| | *Δ* [mm] | *F* [kN] | *Δ* [mm] | *F* [kN] | *Δ* [mm] | *F* [kN] | *Δ* [mm] | *F* [kN] | *Δ* [mm] | *F* [kN] | *Δ* [mm] | *F* [kN] |
| MAX | 0.04 | 13.82 | 0.04 | 14.13 | 0.04 | 14.13 | 0.04 | 14.13 | 0.05 | 14.14 | 0.05 | 14.14 |
| SLS | 0.48 | 6.52 | 0.49 | 8.09 | 0.58 | 8.15 | 0.48 | 6.54 | 0.47 | 6.54 | 0.47 | 6.54 |
| ULS | 2.10 | 8.05 | 2.10 | 8.78 | 2.52 | 8.78 | 2.10 | 8.41 | 2.22 | 8.42 | 2.17 | 8.42 |

The comparison of the results in Table 2 shows that the simplified analysis slightly overestimates the stiffness in the pre-crack region, where the nonlinear analysis is much closer to the experimental results as it considers multilinear behavior in tensions prior reaching the tensile strength (see Fig. **2** b)). In terms of the maximum load, only the simplified analysis with Variant 1 slightly deviates from the averaged experimentally determined maximum load. The variants V2-V4 appear to give a better match. However, it should be noted that the maximum loads for variants V2-V4 was calculated directly with the averaged experimentally determined flexural tensile strength. In contrast, for Variant 1, the tensile strength was calculated by an inverse analysis (see [14] for explanation) and then transformed to the flexural tensile strength with Equation 10.

The SLS and ULS results in Table 2 confirm that the simplified analysis variants V1 and V4 give the best results in terms of matching with the experimental results. The results of variants V2 and V3 indicate that the simplified expressions (Equations 11 and 12) from the fib Model Code for Concrete Structures 2010 [18] for determining the strength values $f_{\mathrm{Fts}}$ and $f_{\mathrm{Ftu}}$ result in relatively inaccurate results for certain fiber-reinforced concrete mixtures (as in this study). Variant 4 also gives a more accurate result for the ULS load. However, it should be noted that this is a consequence of using the same expressions (Equations 4, 5 and 6) to determine the residual tensile strength from the experimental load result and the ULS load from the residual tensile strengths. It can be concluded that the simplified analysis with variant V4 is the most favorable, with regards to its simplicity and matching results –variant V1, which also gives reasonably accurate results, was based on results determined iteratively with the inverse analysis of the experimental results, which has a different (lower) level of simplicity.

## 3 Analysis of Three-Point Bending Tests of Unnotched Polymer Fiber-Reinforced Concrete Prisms

The notched prisms analyzed in Chapter 1 present a rather unpractical option for actual fiber-reinforced concrete elements. It was, therefore, decided to perform the same calculations on a range of unnotched fiber-reinforced concrete prisms with different cross-section heights (from 25 mm to 250 mm by incrementally increasing the height by 25 mm). All other material and geometric properties were the same as in Chapter 1. In terms of calculation, the only difference was that $h_{\mathrm{sp}}$ was equal to $h$ and the deflection calculation according to Equation 3 was disregarded (the prisms were unnotched). Based on the comparison of results in Chapter 2, it was assumed that the nonlinear semi-numeric analysis accurately describes the load-displacement behavior of the analyzed fiber-reinforced concrete prisms and the simplified analysis results were evaluated by comparing them to the nonlinear semi-numeric analysis results. The nonlinear semi-numeric calculation was performed as briefly outlined in Chapter 2 (explained in detail in [14]). The moment-curvature results (an interim calculation of the nonlinear semi-numeric analysis) are shown in Fig. **7**.

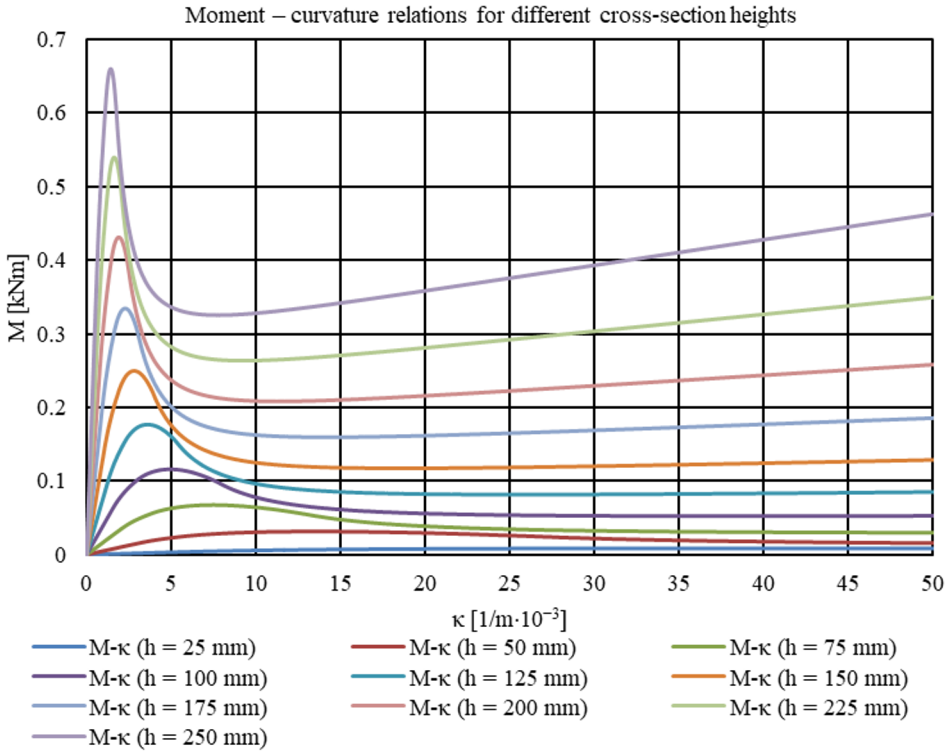


**Fig. 7.** Moment-curvature relations for unnotched fiber-reinforced prisms with different heights.

The moment-curvature results in Fig. **7** give information about the maximum load and loads corresponding to the crack widths ($w$) of interest as they are assumed to be related to strain ($\varepsilon$) according to the relation:

$$\varepsilon = \frac{w}{l_{cs}}, \tag{13}$$

where $l_{cs}$ is the characteristic structural length, considered equal to the cross-section height for elements without conventional reinforcement. The considered crack widths ($w$) were the CTOD values of 0.42 mm and 2.08 mm.

The results of the nonlinear semi-numeric analysis and the simplified analysis are collected in the form of load-displacement charts in Fig. **8**.

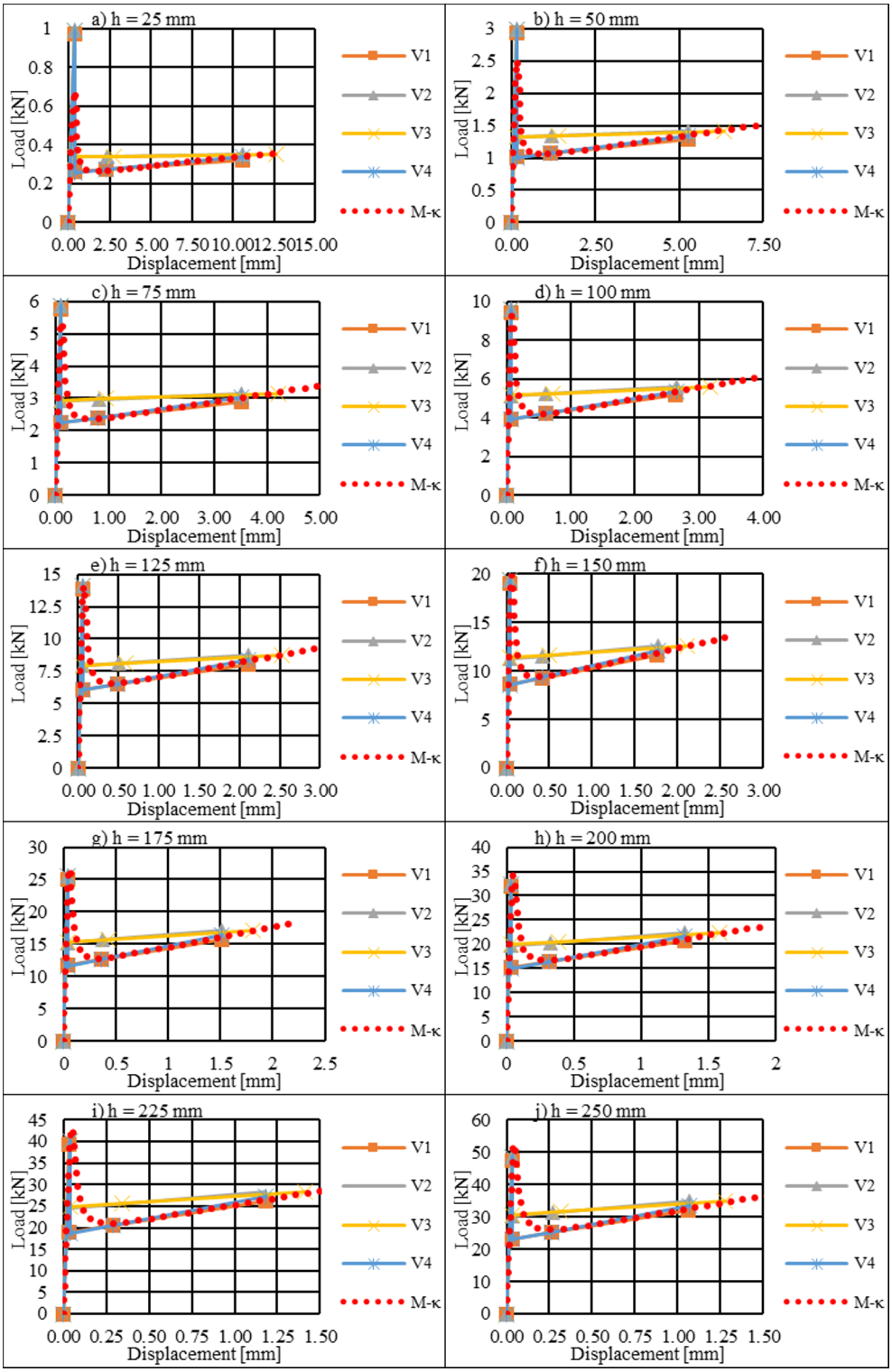


**Fig. 8.** Load-displacement results for the unnotched prisms (for different cross-section heights).

Similarly to the results of the notched prisms, the same conclusions can be drawn for the unnotched prisms: the most accurate (in terms of matching the nonlinear semi-numeric analysis results) are the simplified analysis Variants 1 and 4.

In Tables 3–12, the load-displacement results at the points of interest are given (Point 1–3 in terms of Fig. **3**). MAX denotes the maximum load and corresponding displacement (Point 1), SLS denotes the serviceability limit state load and displacement (Point 2) and ULS denotes the ultimate limit state load and displacement (Point 3).

**Table 3.** Analysis results for the unnotched prism with a cross-section height of 25 mm.

| | **V1** | | **V2** | | **V3** | | **V4** | | **M-κ** | |
|---|---|---|---|---|---|---|---|---|---|---|
| | *Δ* [mm] | *F* [kN] | *Δ* [mm] | *F* [kN] | *Δ* [mm] | *F* [kN] | *Δ* [mm] | *F* [kN] | *Δ* [mm] | *F* [kN] |
| MAX | 0.40 | 0.97 | 0.41 | 0.99 | 0.41 | 0.99 | 0.41 | 0.99 | 0.40 | 0.68 |
| SLS | 2.30 | 0.27 | 2.35 | 0.34 | 2.77 | 0.34 | 2.31 | 0.27 | 2.30 | 0.27 |
| ULS | 10.55 | 0.32 | 10.56 | 0.35 | 12.65 | 0.35 | 10.56 | 0.34 | 10.88 | 0.34 |

**Table 4.** Analysis results for the unnotched prism with a cross-section height of 50 mm.

| | **V1** | | **V2** | | **V3** | | **V4** | | **M-κ** | |
|---|---|---|---|---|---|---|---|---|---|---|
| | *Δ* [mm] | *F* [kN] | *Δ* [mm] | *F* [kN] | *Δ* [mm] | *F* [kN] | *Δ* [mm] | *F* [kN] | *Δ* [mm] | *F* [kN] |
| MAX | 0.15 | 2.93 | 0.16 | 3.00 | 0.16 | 3.00 | 0.16 | 3.00 | 0.17 | 2.51 |
| SLS | 1.18 | 1.07 | 1.20 | 1.34 | 1.42 | 1.34 | 1.18 | 1.08 | 1.17 | 1.06 |
| ULS | 5.28 | 1.29 | 5.28 | 1.40 | 6.32 | 1.40 | 5.28 | 1.35 | 5.48 | 1.37 |

**Table 5.** Analysis results for the unnotched prism with a cross-section height of 75 mm.

| | **V1** | | **V2** | | **V3** | | **V4** | | **M-κ** | |
|---|---|---|---|---|---|---|---|---|---|---|
| | *Δ* [mm] | *F* [kN] | *Δ* [mm] | *F* [kN] | *Δ* [mm] | *F* [kN] | *Δ* [mm] | *F* [kN] | *Δ* [mm] | *F* [kN] |
| MAX | 0.09 | 5.75 | 0.09 | 5.88 | 0.09 | 5.88 | 0.09 | 5.88 | 0.11 | 5.39 |
| SLS | 0.80 | 2.39 | 0.81 | 2.97 | 0.96 | 2.99 | 0.80 | 2.39 | 0.79 | 2.37 |
| ULS | 3.52 | 2.90 | 3.52 | 3.16 | 4.22 | 3.16 | 3.52 | 3.03 | 3.67 | 3.06 |

**Table 6.** Analysis results for the unnotched prism with a cross-section height of 100 mm.

| | **V1** | | **V2** | | **V3** | | **V4** | | **M-κ** | |
|---|---|---|---|---|---|---|---|---|---|---|
| | *Δ* [mm] | *F* [kN] | *Δ* [mm] | *F* [kN] | *Δ* [mm] | *F* [kN] | *Δ* [mm] | *F* [kN] | *Δ* [mm] | *F* [kN] |
| MAX | 0.07 | 9.39 | 0.07 | 9.59 | 0.07 | 9.59 | 0.07 | 9.59 | 0.08 | 9.28 |
| SLS | 0.61 | 4.20 | 0.62 | 5.22 | 0.73 | 5.26 | 0.61 | 4.22 | 0.59 | 4.20 |
| ULS | 2.64 | 5.15 | 2.64 | 5.62 | 3.17 | 5.62 | 2.64 | 5.38 | 2.77 | 5.41 |

**Table 7.** Analysis results for the unnotched prism with a cross-section height of 125 mm.

| | **V1** | | **V2** | | **V3** | | **V4** | | **M-κ** | |
|---|---|---|---|---|---|---|---|---|---|---|
| | *Δ* [mm] | *F* [kN] | *Δ* [mm] | *F* [kN] | *Δ* [mm] | *F* [kN] | *Δ* [mm] | *F* [kN] | *Δ* [mm] | *F* [kN] |
| MAX | 0.05 | 13.82 | 0.05 | 14.13 | 0.05 | 14.13 | 0.05 | 14.13 | 0.07 | 14.14 |
| SLS | 0.49 | 6.52 | 0.50 | 8.09 | 0.59 | 8.15 | 0.49 | 6.54 | 0.48 | 6.54 |
| ULS | 2.11 | 8.05 | 2.12 | 8.78 | 2.53 | 8.78 | 2.12 | 8.41 | 2.22 | 8.42 |

**Table 8.** Analysis results for the unnotched prism with a cross-section height of 150 mm.

| | **V1** | | **V2** | | **V3** | | **V4** | | **M-κ** | |
|---|---|---|---|---|---|---|---|---|---|---|
| | *Δ* [mm] | *F* [kN] | *Δ* [mm] | *F* [kN] | *Δ* [mm] | *F* [kN] | *Δ* [mm] | *F* [kN] | *Δ* [mm] | *F* [kN] |
| MAX | 0.05 | 19.04 | 0.05 | 19.46 | 0.05 | 19.46 | 0.05 | 19.46 | 0.06 | 19.97 |
| SLS | 0.41 | 9.32 | 0.42 | 11.56 | 0.50 | 11.65 | 0.41 | 9.34 | 0.40 | 9.40 |
| ULS | 1.76 | 11.59 | 1.77 | 12.64 | 2.11 | 12.64 | 1.76 | 12.11 | 1.86 | 12.08 |

**Table 9.** Analysis results for the unnotched prism with a cross-section height of 175 mm.

| | **V1** | | **V2** | | **V3** | | **V4** | | **M-κ** | |
|---|---|---|---|---|---|---|---|---|---|---|
| | *Δ* [mm] | *F* [kN] | *Δ* [mm] | *F* [kN] | *Δ* [mm] | *F* [kN] | *Δ* [mm] | *F* [kN] | *Δ* [mm] | *F* [kN] |
| MAX | 0.04 | 25.03 | 0.04 | 25.58 | 0.04 | 25.58 | 0.04 | 25.58 | 0.05 | 26.76 |
| SLS | 0.36 | 12.60 | 0.37 | 15.61 | 0.43 | 15.75 | 0.36 | 12.63 | 0.35 | 12.77 |
| ULS | 1.51 | 15.77 | 1.52 | 17.20 | 1.81 | 17.20 | 1.51 | 16.48 | 1.60 | 16.39 |

**Table 10.** Analysis results for the unnotched prism with a cross-section height of 200 mm.

| | **V1** | | **V2** | | **V3** | | **V4** | | **M-κ** | |
|---|---|---|---|---|---|---|---|---|---|---|
| | *Δ* [mm] | *F* [kN] | *Δ* [mm] | *F* [kN] | *Δ* [mm] | *F* [kN] | *Δ* [mm] | *F* [kN] | *Δ* [mm] | *F* [kN] |
| MAX | 0.04 | 31.79 | 0.04 | 32.49 | 0.04 | 32.49 | 0.04 | 32.49 | 0.05 | 34.49 |
| SLS | 0.32 | 16.35 | 0.33 | 20.25 | 0.38 | 20.44 | 0.32 | 16.40 | 0.31 | 16.67 |
| ULS | 1.33 | 20.60 | 1.33 | 22.46 | 1.59 | 22.46 | 1.33 | 21.52 | 1.41 | 21.34 |

**Table 11.** Analysis results for the unnotched prism with a cross-section height of 225 mm.

| | **V1** | | **V2** | | **V3** | | **V4** | | **M-κ** | |
|---|---|---|---|---|---|---|---|---|---|---|
| | *Δ* [mm] | *F* [kN] | *Δ* [mm] | *F* [kN] | *Δ* [mm] | *F* [kN] | *Δ* [mm] | *F* [kN] | *Δ* [mm] | *F* [kN] |
| MAX | 0.03 | 39.31 | 0.04 | 40.18 | 0.04 | 40.18 | 0.04 | 40.18 | 0.04 | 43.17 |
| SLS | 0.29 | 20.57 | 0.29 | 25.47 | 0.35 | 25.72 | 0.29 | 20.63 | 0.27 | 21.08 |
| ULS | 1.18 | 26.07 | 1.18 | 28.43 | 1.41 | 28.43 | 1.18 | 27.24 | 1.26 | 26.94 |

**Table 12.** Analysis results for the unnotched prism with a cross-section height of 250 mm.

| | **V1** | | **V2** | | **V3** | | **V4** | | **M-κ** | |
|---|---|---|---|---|---|---|---|---|---|---|
| | *Δ* [mm] | *F* [kN] | *Δ* [mm] | *F* [kN] | *Δ* [mm] | *F* [kN] | *Δ* [mm] | *F* [kN] | *Δ* [mm] | *F* [kN] |
| MAX | 0.03 | 47.58 | 0.03 | 48.64 | 0.03 | 48.64 | 0.03 | 48.64 | 0.04 | 52.79 |
| SLS | 0.26 | 25.26 | 0.27 | 31.25 | 0.31 | 31.58 | 0.26 | 25.34 | 0.25 | 26.02 |
| ULS | 1.06 | 32.19 | 1.07 | 35.10 | 1.27 | 35.10 | 1.07 | 33.63 | 1.13 | 33.17 |

The comparison of results in Tables 3–12 confirms the findings of the analysis of the notched prisms in Chapter 2. The most accurate variants of the simplified analysis are the Variant 1 and Variant 4. Even for concrete prisms heights different from the primary (notched) height of 125 mm, Variant 4 gives ULS loads comparably (relative to Variant 1) closer to the nonlinear semi-numeric analysis ULS loads. Note that Equations 4, 5 and 6 were used to determine the residual tensile strengths for the serviceability and ultimate state from a cross-section height of 125 mm, and the same equations were then used to calculate the SLS and ULS loads for different cross-section heights. However, the Variant 4 is especially favorable due to its simplicity. The comparison of the maximum loads indicates that the expression for transforming the tensile strength of concrete to the flexural tensile strength of concrete (Equation 10) gives unreliable (too high) load-bearing capacities for prism heights below 125 mm. In comparison, for heights above 125 mm, the expression gives conservative results.

## 4 Conclusion

This paper presented a simplified analysis for evaluating the load-displacement behavior of fiber-reinforced concrete elements under three-point bending test conditions. Four variants of input tensile strength properties and crack widths, considered for the serviceability and

ultimate limit state, were considered for the simplified analysis. The simplified analysis was evaluated on the notched polymer fiber-reinforced concrete prism three-point bending test results from the study [14] and compared to the nonlinear semi-numeric analysis results from the same study. Additionally, the simplified analysis and the nonlinear semi-numeric analysis were used to determine the load-displacement behavior of unnotched polymer fiber-reinforced concrete prisms with heights ranging from 25 mm to 250 mm. The following conclusions could be drawn from the present research:

- The simplified analysis variants V2 and V3, which used simplified expressions for determining the residual tensile strengths for the serviceability and ultimate limit state, resulted in relatively less accurate load-displacement results. Variant V3 was even less accurate than Variant 2 as it considers the crack mouth opening displacements for the crack widths.
- The simplified analysis variants V1 and V4 relatively accurately described the load-displacement behavior of notched and unnotched polymer fiber-reinforced prisms. However, Variant 4 is especially favorable due to its simplicity (compared to Variant 1, which used tensile strength properties determined with an iterative inverse analysis). The ULS load of Variant 4 was also more accurate (closer to the nonlinear semi-numeric analysis result) than Variant 1.
- The maximum load-bearing capacities calculated with the simplified analysis based on the flexural tensile strength of concrete determined from the tensile strength of concrete (by an expression from the fib Model Code for Concrete Structures 2010 [18]) overestimated the actual maximum load-bearing capacities (evaluated by the nonlinear semi-numeric analysis) for prisms heights bellow 125 mm.

This research was funded by the Slovenian Research and Innovation Agency (project number Z2-4425).

## References

1. O. Ozturk and N. Ozyurt, Journal of Cleaner Production **363**, 132582 (2022)
2. P. Bílý, J. Fládr, P. Ryjáček, and V. Stančík, Bridge Structures **16**, 15 (2020)
3. C. Camille, D. K. Hewage, O. Mirza, F. Mashiri, B. Kirkland, and T. Clarke, Construction and Building Materials **270**, 121469 (2021)
4. P. wei Jiang, J. hua Fang, J. yong Pang, Q. Su, and X. Xia, Arabian Journal for Science and Engineering **45**, 8655 (2020)
5. Materials and Structures **35**, 262 (2002)
6. C. Pedersen, New Production Processes, Materials and Calculation Techniques for Fibre Reinforced Pipes, Doctoral Thesis, Technical University of Denmark, Kongens Lyngby, 1996
7. P. Casanova and P. Rossi, Structural Journal **94**, 595 (1997)
8. H. Stang and J. F. Olesen, in *FRAMCOS-3* (Aedificatio Publishers, 1998), pp. 511–520
9. C. Soranakom and B. Mobasher, Journal of Engineering Mechanics **133**, 933 (2007)
10. G. Volpatti, J. A. Martínez, J. C. Diaz, and D. Zampini, Composite Structures **279**, 114755 (2022)
11. J. Zhang and H. Stang, Cement and Concrete Research **28**, 439 (1998)
12. D.-Y. Yoo, Y.-S. Yoon, and N. Banthia, Construction and Building Materials **93**, 477 (2015)
13. Ž. Unuk and M. Kuhta, Buildings **12**, 2143 (2022)

14. Ž. Unuk and M. Kuhta, Applied Sciences **14**, 1604 (2024)
15. European Committee for Standardization, (2004)
16. Barchip, Https://Barchip.Com/Product/ (2024)
17. European Committee for Standardization, (2006)
18. Fédération internationale du béton, *Fib Model Code for Concrete Structures 2010* (2013)
19. H. Tada, P. C. Paris, and G. R. Irwin, *The Stress Analysis of Cracks Handbook*, 3rd ed. (ASME Press, New York, 2000)
20. M. Di Prisco, M. Colombo, and D. Dozio, Structural Concrete **14**, 342 (2013)
21. European Committee for Standardization, (2007)